



This is a repository copy of *A novel interface constitutive model for prediction of stiffness and strength in 3D braided composites.*

White Rose Research Online URL for this paper:
<http://eprints.whiterose.ac.uk/112044/>

Version: Accepted Version

Article:

Zhang, C., Curiel-Sosa, J.L. and Bui, T.Q. (2017) A novel interface constitutive model for prediction of stiffness and strength in 3D braided composites. *Composite Structures*, 163. pp. 32-43. ISSN 0263-8223

<https://doi.org/10.1016/j.compstruct.2016.12.042>

Reuse

Unless indicated otherwise, fulltext items are protected by copyright with all rights reserved. The copyright exception in section 29 of the Copyright, Designs and Patents Act 1988 allows the making of a single copy solely for the purpose of non-commercial research or private study within the limits of fair dealing. The publisher or other rights-holder may allow further reproduction and re-use of this version - refer to the White Rose Research Online record for this item. Where records identify the publisher as the copyright holder, users can verify any specific terms of use on the publisher's website.

Takedown

If you consider content in White Rose Research Online to be in breach of UK law, please notify us by emailing eprints@whiterose.ac.uk including the URL of the record and the reason for the withdrawal request.



eprints@whiterose.ac.uk
<https://eprints.whiterose.ac.uk/>

Accepted Manuscript

A novel interface constitutive model for prediction of stiffness and strength in 3D braided composites

Chao Zhang, J.L. Curiel-Sosa, Tinh Quoc Bui

PII: S0263-8223(16)31766-4

DOI: <http://dx.doi.org/10.1016/j.compstruct.2016.12.042>

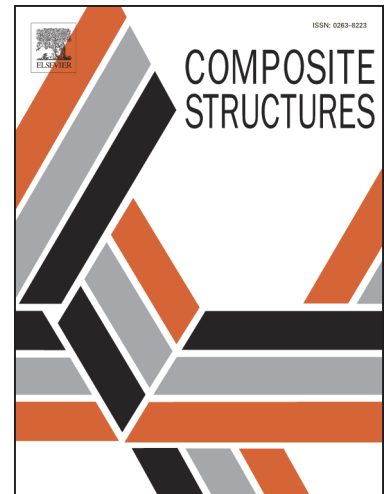
Reference: COST 8097

To appear in: *Composite Structures*

Received Date: 5 September 2016

Revised Date: 27 November 2016

Accepted Date: 9 December 2016



Please cite this article as: Zhang, C., Curiel-Sosa, J.L., Quoc Bui, T., A novel interface constitutive model for prediction of stiffness and strength in 3D braided composites, *Composite Structures* (2016), doi: <http://dx.doi.org/10.1016/j.compstruct.2016.12.042>

This is a PDF file of an unedited manuscript that has been accepted for publication. As a service to our customers we are providing this early version of the manuscript. The manuscript will undergo copyediting, typesetting, and review of the resulting proof before it is published in its final form. Please note that during the production process errors may be discovered which could affect the content, and all legal disclaimers that apply to the journal pertain.

A novel interface constitutive model for prediction of stiffness and strength in 3D braided composites

Chao Zhang^{a,*}, JL Curiel-Sosa^b, Tinh Quoc Bui^c

^aSchool of Mechanical Engineering, Jiangsu University, Zhenjiang, China

^bDepartment of Mechanical Engineering, The University of Sheffield, Sheffield, UK

^cDepartment of Civil and Environmental Engineering, Tokyo Institute of Technology, Tokyo, Japan

*Corresponding author: Chao Zhang, E-mail: zhangchao@ujs.edu.cn, Tel: +86 511 88780169, Fax: +86 511 88790627, Department of Mechanical Design, 301 Xuefu Road, Zhenjiang, 212013, Jiangsu, China

Abstract: Owing to the excellent integrated mechanical properties, 3D braided composites have a broad range of engineering applications in aeronautics and astronautics industry. The interface is a critical constituent of 3D braided composites, which plays an important role in the control of mechanical properties of the composites. In this paper, a meso-scale finite element model considering the interface is established to numerically predict the stiffness and strength properties of 3D braided composites. A novel damage-friction combination interface constitutive model is utilized to capture the interface debonding behavior, while 3D Hashin criteria with Maximum stress criteria and a gradual degradation scheme are applied to predict the damage evolution of yarns and matrix. A user-material subroutine VUMAT based on finite element package ABAQUS/Explicit is developed for these constitutive models. The stiffness and strength properties of 3D braided composites are derived from the calculated stress-strain curves under typical loading cases. The damage mechanism of constituents especially the interface is revealed in these simulation processes. The effects of the interface parameters on the mechanical properties of composites are investigated, which provides a reference for optimizing design and control of the interface properties of 3D braided composites.

Keywords: 3D braided composites; stiffness properties; strength properties; frictional cohesive interface; finite element analysis

1 Introduction

3D braided composites are a kind of textile composites that are manufactured by braided preforms impregnated and consolidated with resin materials. The yarns of 3D braided composites are intertwined to form the spatial near-net-shape structure, which can fundamentally overcome the fatal shortcomings of low inter-laminar strength and low delamination resistance of conventional laminated composites. Moreover, the excellent integrated mechanical properties of 3D braided composites highly meet the requirements of aerospace structural materials for weight reduction and high load-bearing capacity. Consequently, 3D braided composites are believed to have broad potential applications as the primary loading-bearing structures in aeronautics and astronautics industry. Before 3D braided composites are used in primary loading-bearing structures, a rational characterization of their stiffness and strength properties is essential.

In general, 3D braided composites are composed of three phases including braiding yarn, resin matrix and interface. Fiber yarn bears the main loads and provides the structural stiffness and strength of the composites. Resin matrix plays a supporting role that fixes the fibers and disperses the loads between the fibers. The interface is the bridge between the braiding yarn and matrix, which determines how the stress is transferred and the distribution between the fiber and matrix and it influences significantly on the damage initiation and propagation in the materials.

Numerous studies on the mechanical properties of 3D braided composites have been made, including the establishment of structural models [1-4], the prediction of stiffness and strength properties [5-9], and the investigation of damage and failure mechanisms under various loadings [10-15]. In these micromechanical analysis works, only two constituents: the braiding yarn and matrix have been considered while the interface has been ignored. However, the interface is a critical constituent of 3D braided composites, and it has a major influence on the control of mechanical properties of the composites. The properties of the interface can be adjusted to obtain better match between the yarn and matrix and achieve the best composite effect. In recent years, with the rapid development of finite element simulation technology and the in-depth study of the micromechanical properties, research on interface behavior of braided composites has attracted much attention.

Fang et al. [16] firstly proposed a unit-cell model involving the interface damage model to predict the progressive damage process of 3D braided composites under uniaxial tensile loading. Xu et al. [17] developed a multi-layers micromechanical model, in which the interfacial mechanical properties could be defined, to predict the elastic modulus of 3D multi-phase braided composites. Lei et al. [18] established a representative unit-cell with interface zones to study the effect of cut-edge on the tensile properties of 3D braided composites by using nonlinear numerical analysis. Lu et al. [19] presented a nonlinear finite element model to investigate the effect of interfacial properties on the uniaxial tensile behavior of 3D braided composites. A cohesive zone model was used to evaluate the debonding behavior of interface between yarn and matrix and the interfacial properties were determined by numerical parametrical study. Xu et al. [20] formulated a cohesive zone model to analyze the fiber push-out problems in metal matrix composites at elevated temperature. In the cohesive zone model, the interfacial debonding and frictional sliding behavior as well as the effect of the residual stress have been considered. Sharma et al. [21] developed an image-based finite element model to determine the homogenized effective elastic properties of 3D carbon/carbon composites. In this model, the imperfections of microstructure such as cracks and

voids, the cross-section distortion and mis-alignment of the yarns were introduced by using X-ray tomography, and the yarn/matrix interfaces were modeled as frictional cohesive surfaces. Similar studies dealing with the interface response of 2D braided composites based on the unit-cell model can be found in references [22-24].

Overall, thus far, the study on the interface behavior of 3D braided composites is relatively limited. Besides, the related research work had not considered the influence of the friction on the interfacial mechanical response and the understanding of interface stress transfer and interface damage mechanisms is insufficient, which needs to be studied further. In this paper, a meso-scale finite element model, in which the yarn/matrix and yarn/yarn interfaces are modeled by cohesive elements, is established to predict the stiffness and strength properties of 3D braided composites. Considering the possible friction appearing on debonding interface under compression loads, a damage-friction combination interface constitutive model is proposed. Then a continuum damage model applied to predict damage evolution of yarns and matrix and this interface constitutive model is coded in the framework of a user-material subroutine VUMAT in ABAQUS/Explicit. The damage initiation and propagation of each constituent in 3D braided composites under typical loading cases are simulated and the stiffness and strength properties are predicted from the calculated stress-strain curves. In addition, the effects of interface stiffness, strength and friction coefficient on the mechanical properties of composites are discussed by a parametric study.

2 Damage constitutive models

2.1 Interface constitutive model

The architecture of 3D braided composites is very complicated thus it is difficult to directly test the interface properties of the composites. On the other hand, the meso-scale finite element modeling can overcome this limitation and it is appropriate for simulating the damage initiation and propagation at the interface. Establishing a reasonable interface constitutive model is the premise for analyzing the interface mechanical behavior of 3D braided composites.

2.1.1 Interface constitutive model without friction

A cohesive element is used to represent the interface debonding in the yarn/matrix and yarn/yarn interfaces of 3D braided composites. The traction stress and separation displacement of the nodes on the interface are governed by traction-separation law. The traction stress on the interface consists of three components: a normal traction and two shear tractions. The constitutive relationship can be described as

$$\begin{Bmatrix} t_1 \\ t_2 \\ t_3 \end{Bmatrix} = \begin{bmatrix} k_1 & 0 & 0 \\ 0 & k_2 & 0 \\ 0 & 0 & k_3 \end{bmatrix} \begin{Bmatrix} \delta_1 \\ \delta_2 \\ \delta_3 \end{Bmatrix} \quad (1)$$

where t is the traction stress, δ is the separation displacement, and k represents the initial stiffness of the interface.

The bi-linear models of cohesive element under typical pure modes are depicted in Fig. 1. The softening initiation displacements, δ_1^0 , δ_2^0 , δ_3^0 , are obtained as

$$\delta_1^0 = \frac{N}{k_1}, \quad \delta_2^0 = \frac{S}{k_2}, \quad \delta_3^0 = \frac{T}{k_3} \quad (2)$$

where N , S and T are the interface tensile and shear strengths, respectively.

The final displacements for the state of complete debonding, δ_1^f , δ_2^f , δ_3^f , are determined by

$$\delta_1^f = \frac{2G_{IC}}{N}, \delta_2^f = \frac{2G_{IIC}}{S}, \delta_3^f = \frac{2G_{IIIC}}{T} \quad (3)$$

where G_{IC} , G_{IIC} and G_{IIIC} are respective critical fracture energies of mode I, II and III.

In general, debonding growth is likely to occur under mixed-mode loading. The mix-mode bilinear constitutive model of interface element is shown in Fig. 2. Herein, it is assumed that $S=T$, $G_{IIC} = G_{IIIC}$ and $k_1 = k_2 = k_3 = K$.

For the mixed-mode, the effective relative displacement, δ_m , is defined as

$$\delta_m = \sqrt{\langle \delta_1 \rangle^2 + \delta_2^2 + \delta_3^2} = \sqrt{\langle \delta_1 \rangle^2 + \delta_{shear}^2} \quad (4)$$

where δ_{shear} represents the norm of the vector defining the tangential relative displacements of the element, and the $\langle x \rangle$ operator is defined by

$$\langle x \rangle = \begin{cases} 0 & x \leq 0 \\ x & x > 0 \end{cases} \quad (5)$$

Defining the mode mixing ratio $\beta = \delta_{shear} / \delta_1$, and using a quadratic nominal stress criterion, the softening initiation displacement under mixed-mode conditions is then obtained following as [25]

$$\delta_m^0 = \begin{cases} \delta_1^0 \delta_{shear}^0 \sqrt{\frac{1+\beta^2}{(\delta_{shear}^0)^2 + (\beta\delta_1^0)^2}} & \delta_1 > 0 \\ \delta_{shear}^0 & \delta_1 \leq 0 \end{cases} \quad (6)$$

In the above equation, when $\beta = 0$, the mixed-mode is reduced to pure mode I and $\delta_m^0 = \delta_1^0$; when $\beta \rightarrow \infty$, the mixed-mode is reduced to shear model and $\delta_m^0 = \delta_{shear}^0 = \delta_2^0$.

Adopting the power interaction law of the energy, the final displacement of mixed-mode is obtained as [25]

$$\delta_m^f = \begin{cases} \frac{2(1+\beta^2)}{K\delta_m^0} \left[\left(\frac{1}{G_{IC}} \right)^2 + \left(\frac{\beta^2}{G_{IIC}} \right)^2 \right]^{-1/2} & \delta_1 > 0 \\ \sqrt{(\delta_2^f)^2 + (\delta_3^f)^2} & \delta_1 \leq 0 \end{cases} \quad (7)$$

In the above equation, when $\beta = 0$, the mixed-mode is reduced to pure mode I and $\delta_m^f = \delta_1^f$; when $\beta \rightarrow \infty$, the mixed-mode is reduced to the shear model and $\delta_m^f = \delta_{shear}^f = \sqrt{(\delta_2^f)^2 + (\delta_3^f)^2}$.

In the finite element analysis, the relative displacement on the interface element is always changing. Considering the irreversibility of damage, the maximum relative displacement, δ_m^{\max} , is defined as

$$\delta_m^{\max} = \max \{ \delta_m^{\max}, \delta_m \} \quad (8)$$

The irreversible bi-linear constitutive equation for mixed-mode is obtained and can be expressed as

$$t_s = D_{sr} \delta_r \quad (s = 1, 2, 3 ; r = 1, 2, 3) \quad (9a)$$

$$D_{sr} = \begin{cases} \bar{\delta}_{sr} K & (\delta_m^{\max} \leq \delta_m^0) \\ \bar{\delta}_{sr} (1-d) K & (\delta_m^0 < \delta_m^{\max} < \delta_m^f, \delta_1 > 0) \\ \bar{\delta}_{sr} [(1-d)K + Kd\bar{\delta}_{s1}] & (\delta_m^0 < \delta_m^{\max} < \delta_m^f, \delta_1 \leq 0) \\ 0 & (\delta_m^{\max} \geq \delta_m^f, \delta_1 > 0) \\ \bar{\delta}_{s1} \bar{\delta}_{1r} K & (\delta_m^{\max} \geq \delta_m^f, \delta_1 \leq 0) \end{cases} \quad (9b)$$

where $\bar{\delta}_{ij}$ is the Kronecker operator. The damage evolution function d is expressed by

$$d = \frac{\delta_m^f (\delta_m^{\max} - \delta_m^0)}{\delta_m^{\max} (\delta_m^f - \delta_m^0)} \quad d \in [0,1] \quad (10)$$

2.1.2 Damage-friction combination interface constitutive model

In this section, a novel damage-friction interface constitutive model is presented. For a representative interface, it is considered that the area A of this representative interface is equal to the sum of the undamaged area A_u and the damaged area A_d , namely

$$A = A_u + A_d = (1-d)A + dA \quad (11)$$

The stress on the representative interface is [26]

$$\tau = (1-d)\tau_u + d\tau_d \quad (12)$$

where τ_u and τ_d are the interface stress on the undamaged area and damaged area, respectively.

In Eq. (9), it is considered that no interface damage is generated when the interface element is under pure compressive load. Additionally, if the interface is damaged, only normal compressive stresses exist on the damaged area of the interface. However, when the interface element is damaged, the interface becomes rough. If the interface is subjected to normal compressive load at this moment, the relative micro-slip of the interface can cause a high friction force on the damaged area.

In this paper, the influence of the friction force on the interface response is considered, and the stress on the representative interface in the Eq. (12) can be rewritten as

$$\tau = \tau_s + \tau_f \quad (13)$$

Here, τ_s is determined by Eq. (9), τ_f is the friction force generated on the damaged interface, and expressed as follows:

$$\tau_{fr} = \begin{cases} \tau_{f1} = 0 & (\delta_1 \geq 0) \\ 0 & (\delta_m^{\max} \leq \delta_m^0, \delta_1 < 0) \\ -\mu K d \delta_1 \delta_r / |\delta_r| & (\delta_m^0 < \delta_m^{\max} < \delta_m^f, \delta_1 < 0) \\ -\mu K \delta_1 \delta_r / |\delta_r| & (\delta_m^{\max} \geq \delta_m^f, \delta_1 < 0) \end{cases} \quad (r = 2, 3) \quad (14)$$

where μ is the interface friction coefficient.

Finally, the damage-friction combination interface constitutive model is established as described in Eq. (13). This interface constitutive model is evaluated by the interface initial stiffness K , the damage evolution function d ,

the interface friction coefficient μ , and the mixed-mode relative displacements corresponding to softening initiation and complete debonding, δ_m^0 and δ_m^f , respectively.

2.2 Constitutive model of yarns and matrix

2.2.1 Damage initiation criteria

In this paper, the 3D Hashin failure criteria [27] and Maximum stress criteria are applied to define the damage initiation of braiding yarns and matrix in the unit-cell model. The Hashin criteria are established in terms of mathematical expressions using material strengths with the consideration of distinct failure modes. For ease of reference, these equations of Hashin criteria are repeated as follows:

Yarn tensile failure in L direction ($\sigma_L \geq 0$)

$$\varphi_{L_t} = \left(\frac{\sigma_L}{F_L^t} \right)^2 + \alpha \left(\frac{\sigma_{LT}}{S_{LT}} \right)^2 + \alpha \left(\frac{\sigma_{LZ}}{S_{LZ}} \right)^2 \geq 1 \quad (15)$$

Yarn compressive failure in L direction ($\sigma_L < 0$)

$$\varphi_{L_c} = \left(\frac{\sigma_L}{F_L^c} \right)^2 \geq 1 \quad (16)$$

Yarn tensile and shear failure in T and Z direction ($\sigma_T + \sigma_Z \geq 0$)

$$\varphi_{T(Z)_t} = \left(\frac{\sigma_T + \sigma_Z}{F_T^t} \right)^2 + \left(\frac{1}{S_{TZ}^2} \right) (\sigma_{TZ}^2 - \sigma_T \sigma_Z) + \left(\frac{\sigma_{LT}}{S_{LT}} \right)^2 + \left(\frac{\sigma_{LZ}}{S_{LZ}} \right)^2 \geq 1 \quad (17)$$

Yarn compressive and shear failure in T and Z direction ($\sigma_T + \sigma_Z < 0$)

$$\varphi_{T(Z)_c} = \left(\frac{\sigma_T + \sigma_Z}{2S_{TZ}} \right)^2 + \left(\frac{\sigma_T + \sigma_Z}{F_T^c} \right) \left[\left(\frac{F_T^c}{2S_{TZ}} \right)^2 - 1 \right] + \frac{1}{S_{TZ}^2} (\sigma_{TZ}^2 - \sigma_T \sigma_Z) + \left(\frac{\sigma_{LT}}{S_{LT}} \right)^2 + \left(\frac{\sigma_{LZ}}{S_{LZ}} \right)^2 \geq 1 \quad (18)$$

In the above equations, F_L^t and F_L^c are the longitudinal tensile and compressive strengths of braiding yarn; F_T^t and F_T^c are the transverse tensile and compressive strengths; S_{LT} , S_{LZ} and S_{TZ} are the LT , LZ and TZ shear strengths, respectively. L - T - Z rectangular coordinate is the local coordinate definition of braiding yarn, and L axis, T axis and Z axis indicate the axial and two transverse directions.

2.2.2 Damage evolution model

Once the damage initiation criteria are satisfied, further loading will cause degradation of material stiffness constants. The reduction of the stiffness constants is controlled by damage variables ranged from 0 (initial undamaged) to 1 (completely damaged) according to the damage situation. Herein, a gradual degradation scheme coupling with Murakami damage model proposed by Lapczyk et al. [28] and Fang et al. [11] is used to characterize the damage evolution of the yarns and matrix.

The evolution of damage variable for each failure mode is determined by

$$d_I = \frac{\delta_{1,eq}^f (\delta_{1,eq}^0 - \delta_{1,eq}^f)}{\delta_{1,eq}^f (\delta_{1,eq}^f - \delta_{1,eq}^0)} \quad (I = Lt, Lc, Tt, Tc, Zt, Zc, Mt, Mc) \quad (19)$$

where $\delta_{1,eq}^0$ is the initial equivalent displacement at which the failure criterion is satisfied. $\delta_{1,eq}^f$ is the full

equivalent displacement at which the material is completely failure. They are defined as

$$\delta_{1,eq}^0 = \delta_{1,eq} / \sqrt{\varphi_1} \quad (20)$$

$$\delta_{1,eq}^f = 2G_1 / (\sigma_{1,eq} / \sqrt{\varphi_1}) \quad (21)$$

Here, φ_1 is the value of damage initiation criterion, G_1 is the fracture energy density. $\delta_{1,eq}$ and $\sigma_{1,eq}$ are the equivalent displacement and stress for a failure mode, respectively.

3 Meso-scale finite element model

3.1 Unit-cell structural model

In this paper, the unit-cell structural model of 3D braided composites proposed by Xu and Xu [3] is employed, which is schematically shown in Fig. 3. The cross-section shape of the braiding yarns is considered as octagon containing an inscribed ellipse. Therefore, the interface zones of yarn/matrix and yarn/yarn are both planes, which is convenient for the introduction of interface and the generation of zero-thickness cohesive elements.

The relationship between the major radius a and minor radius b of the ellipse and interior braiding angle γ of 3D braided composites, is expressed as

$$a = \sqrt{3}b \cos \gamma \quad (22)$$

W_x , W_y and h represent the width, thickness and height of the unit-cell model respectively, and they can be computed by:

$$W_x = 4\sqrt{2}b \quad (23)$$

$$W_y = 4\sqrt{2}b \quad (24)$$

$$h = 8b / \tan \gamma \quad (25)$$

In the following numerical calculation, the structural parameters of the unit-cell model are given as follows: $\gamma=46.4^\circ$, $W_x=W_y=1.662\text{mm}$, $h=2.238\text{mm}$, $V_f=52\%$. Obviously, the unit-cell model here is with a typical large braiding angle.

3.2 Boundary conditions

Since the finite element analysis is based on the unit-cell modeling, periodic boundary conditions should be applied to replicate the repeating nature. As proposed by Xia et al [29], the displacements on a pair of parallel opposite boundary surfaces (denoted as “j+” and “j-”) of a unit-cell model can be expressed as

$$u_i^{j+} = \bar{\varepsilon}_{ik} x_k^{j+} + u_i^* \quad (26)$$

$$u_i^{j-} = \bar{\varepsilon}_{ik} x_k^{j-} + u_i^* \quad (27)$$

In the above equations, $\bar{\varepsilon}_{ik}$ are the average strains of the unit-cell, x_k is the Cartesian coordinate of a unit-cell point and u_i^* is the periodic part of the displacement components on the boundary surfaces.

For a unit-cell, u_i^* is same at the two parallel boundaries. The difference between the above two equations can be written as

$$u_i^{j+} - u_i^{j-} = \bar{\epsilon}_{ik} (x_k^{j+} - x_k^{j-}) = \bar{\epsilon}_{ik} \Delta x_k^j \quad (28)$$

where Δx_k^j are constants for each pair of boundary surfaces. And once $\bar{\epsilon}_{ik}$ is specified, the right side of Eq. (28) becomes constant.

As a special form of displacement boundary conditions, Eq. (28) can be carried out easily in the finite element analysis by setting the nodal displacement constraint equations. The detailed application process can be found in the reference [30-31].

3.3 Mesh discretization

In this paper, the interface in the yarn/matrix and yarn/yarn zones is introduced in the unit-cell model to study the interfacial behavior of 3D braided composites. However, due to the complicated microstructure of 3D braided composites, mesh generation becomes a very difficult and challenging task. Herein, 3D solid tetrahedral element (C3D4) available in ABAQUS is adopted for the discretization of yarns and matrix because of its excellent geometry adaptability. Since the thickness of interface is extremely thin, it is not trivial to generate cohesive elements in a so complex microstructure directly by general finite element software or mesh generation tools. Therefore, a FORTRAN pre-compiler code involving the cohesive elements generation is developed and implemented to modify the INP model file of ABAQUS. Through this way, the zero-thickness cohesive elements are introduced in the unit-cell model of 3D braided composites. Since C3D4 elements are used for meshing yarns and matrix, the element type of interfacial element must be 6-node 3D cohesive element (COH3D6) for nodes consistent. The finite element mesh of unit-cell of 3D braided composites is shown in Fig. 4. Different parameters can be assigned to the yarn/matrix and yarn/yarn interface to express different interfacial mechanical properties. In this paper, the interface parameters in these two zones are same. The unit-cell model consists of 11, 143 nodes, 40, 811 C3D4 elements and 5, 926 COH3D6 elements.

3.4 Material properties of constituents

3D braided composites are composed of braiding yarns, resin matrix and interface. The material response of the constituents directly influences the macro-mechanical behavior of the composites. The braiding yarn containing thousands of fibers and matrix is considered as transversely isotropic material in the local material coordinate system after resin impregnation, and the resin matrix is assumed to be isotropic material. For the local coordinate definition of braiding yarn in a specify orientation, local 1-axis follows the yarn centerline and local 3-axis is in the upright plane perpendicular to the x - y plane of the global coordinate, as shown in Fig. 3(b). The micromechanics formulae proposed by Chamis [32] are selected to compute the stiffness and strength properties of the impregnated yarn in the unit-cell model. The material properties of fiber and matrix cited from Ref. [11] are listed in Table 1, and the appropriate interface properties are summarized in Table 2.

3.5 Prediction of stiffness and strength properties

To obtain the macroscopic mechanical properties of the composites, the homogenization approach is employed. The heterogeneous composites in the micro-scale are regarded as a homogeneous material in the macro-scale. The average stresses and strains in a unit-cell are defined by

$$\bar{\sigma}_{ij} = \frac{1}{V} \int_V \sigma_{ij} dV \quad \bar{\varepsilon}_{ij} = \frac{1}{V} \int_V \varepsilon_{ij} dV \quad (29)$$

where V is the volume of the unit-cell.

The unit-cell is considered as anisotropic materials, and the stress-strain relationship can be determined by

$$\bar{\sigma}_i = E_{ij} \bar{\varepsilon}_j \quad (30)$$

where E_{ij} is the effective stiffness matrix.

In the cuboid unit-cell, global average strain $\bar{\varepsilon}_{ij}$ is applied by periodic boundary conditions in the finite element analysis. For global average stress $\bar{\sigma}_{ij}$, it is related to the ratios of resultant traction force on the boundary surface to corresponding area of the boundary surface, namely

$$\bar{\sigma}_{ij} = (P_i)_j / S_j \quad (31)$$

In the above equation, $(P_i)_j$ is the i th resultant forces on the j th boundary surface and S_j is the area of the j th boundary surface.

The elastic properties of 3D braided composites are predicted from the initial linear segments of the computed stress-strain curves, namely

$$E_i = \frac{\bar{\sigma}_i}{\bar{\varepsilon}_i}, \quad \mu_{ij} = -\frac{\bar{\varepsilon}_i}{\bar{\varepsilon}_j}, \quad G_{ij} = \frac{\bar{\sigma}_{ij}}{\bar{\varepsilon}_{ij}} \quad (i, j=1, 2, 3) \quad (32)$$

Lastly, the strength properties are determined as maximum stresses of the computed stress-strain curves.

3.6 Numerical analysis process

The constitutive model of each constituent and the progressive damage simulation approach are implemented into a user-defined material subroutine VUMAT, available in finite element software ABAQUS. During each time increment, ABAQUS transmits the information of strain increment to VUMAT. With the constitutive models, the stress level and damage state in each constituent of the unit-cell can be obtained. Once the failure criterion is satisfied, the material properties reduction is carried out by updating the damage variables. The stresses at the integration points of elements are updated by the reduced stiffness matrix. Finally, the updated state variables are returned to ABAQUS for next step analysis. The flow chart of whole numerical analysis process is briefly represented in Fig. 5.

4 Numerical results and discussions

Due to the spatial rotation characteristics of braiding yarns in 3D braided composites, the stiffness properties, strength properties and damage characteristics of the unit-cell model under x and y tension, as well as under xz and yz shear, are similar. Accordingly, in this work, only the numerical results of the unit-cell model under z tension, x tension, xy shear and xz shear are given.

4.1 ABAQUS/Explicit quasi-static analysis

In this paper, we first try to use ABAQUS/Standard to perform the static mechanical analysis of the unit-cell

model. However, we have found that when the interface elements are seriously damaged, the convergence of computation will be deteriorated and sometimes the numerical calculation will be terminated before the stress-strain curve reach the maximum stress. By introducing the viscosity coefficient and reducing the increment of each step, the convergence gets better, but it is difficult to avoid the termination of computation. This situation also appears in the related research work involving cohesive elements by using implicit solver, e.g., see [16, 18-19]. A switching explicit-implicit solver [33-34] could prove convenient although this has not been attempted in this work. Thus, in order to improve the convergence of numerical computation, the quasi-static analysis of the unit-cell model is carried out by using ABAQUS/Explicit. Under all the typical loading cases, the strains are 1.5%-2% and the load time is 0.001s. By evaluating various energies generated in the computation process, the kinetic energy of the composites accounted for less than 1% of the internal energy, much less than the experience value of 5%-10%, which can ensure the "real" quasi-static of the solution.

4.2 Preliminary validation of the interface constitutive model

Herein, to validate the damage-friction combination interface constitutive model, only the damage of interface elements is introduced by VUMAT subroutine in ABAQUS/Explicit first. Due to the absence of experimental and numerical results considering friction effect, the friction coefficient is set as 0 here. Then Eq. (13) is exactly reduced to Eq. (9) as the interface constitutive model without considering the friction. Under this condition, for the same unit-cell model of 3D braided composites, the numerical results obtained from cohesive constitutive model available in ABAQUS and VUMAT subroutine developed in this paper are compared, as shown in Fig. 6. With the same strain loading under z tension $\bar{\epsilon}_z = 0.92\%$, the stress state and damage distribution of interface elements are very close to each other. Furthermore, the x tension, xy shear and xz shear loads are applied to the unit-cell model and the numerical results are compared. It is observed that the comparison results are always consistent when subjected to the same loading conditions, which preliminarily verifies the interface damage constitutive model coded in the VUMAT subroutine.

4.3 Stress-strain curves

The stress-strain curves illustrate the macroscopic mechanical behavior of 3D braided composites under corresponding loadings. In experiments, the carbon-fiber reinforced composites specimens tend to exhibit brittle breaking characteristics and the experimental stress-strain curves always stop after reaching the maximum stresses. However, the computed stress-strain curves provide the whole simulation process from damage initiation, propagation to catastrophic failure. As shown in Fig. 7, the stress-strain curves of 3D braided composites specimen under different loading cases keep linear before the initiation of damage. With the occurrence, accumulation and coupling of different damage modes, the stress-strain curves become to be nonlinear. After reaching the maximum stresses, the computed curves decrease rapidly or gradually according to the loading cases and then the materials loss the carrying capacity. The extended unloading observed in the computed stress-strain curves is considered as a numerical artifact because the experimental specimens most likely have more brittle failure, whereas the computed curves have more gradual unloading to promote numerical stability [23]. In addition, it can be found that there is a "rebound area" on the z tension stress-strain curve at strain 1.12% and it also exists on the x tension stress-strain curve at strain 1.21%. This may be due to the interface debonding which

causes a tendency of the angle between fiber direction and loading direction to be smaller. Then, because of the interaction of other damage modes of braiding yarn and matrix, the curve decreases gradually after a slightly increase. Under z tension, xy shear and xz shear, the interface damage occurs first and the yarn damage occurs afterwards while it is opposite under x tension. However, the matrix damage always appears lastly under these four loading cases.

All the predicted stiffness and strength properties are given in Table 3. From Table 3, it is seen that the unit-cell model is almost perfect transversely isotropic. That is the reason why the stress-strain curves under y tension and yz shear are not given here.

4.4 Damage mechanism analysis

The advantage of the proposed meso-scale modeling strategy is that the detailed information on the stress distribution and damage mechanism in the 3D braided composites under different loadings can be obtained. The damage evolution process of interface elements in the unit-cell model, which is especially concerned in this paper, is illustrated in Fig. 8. The failure mode and damage mechanism are different under different loading cases. Under z tension load, the main failure modes are yarn T compressive shear failure, yarn Z tensile shear failure, matrix cracking and interface debonding. As shown in Fig. 8(a), at $\bar{\epsilon}_z = 0.35\%$, the interface damage occurs first in the yarn/yarn contact zones near the top and bottom surfaces of the unit-cell. Due to the spatial rotation symmetry of braiding yarns in the unit-cell model, it can provide relatively balanced load-bearing of the braiding yarns and interface elements under tension load. With the increase of z tensile load, the interface damage in the yarn/yarn contact zones is progressively expanded along the fiber axial and transverse directions and the expansion rate is gradually accelerated. After $\bar{\epsilon}_z = 0.71\%$, the interface damage occurs in the yarn/matrix contact zones and the damage area is increasingly extended along the fiber axial direction. In conclusion, under z tension, the yarn/yarn contact zones are the most serious damage regions, and both the normal stress component and shear stress component contribute to the damage evolution of interface.

Under x tension load, the main failure modes of the braided composites are yarn T tensile shear failure and matrix cracking. Z tensile shear failure occurs in some elements in the braiding yarn, but the quantity is relatively small. As shown in Fig. 8(b), the interface damage occurs first in the yarn/yarn contact zones near the boundary surfaces of the unit-cell. However, the number of damaged interface elements is small and the expansion rate of interface damage is relatively slow. This is because the interface strength in numerical calculation is relatively large and the generation of transverse damage of braiding is more easily than that of the interface debonding.

Under xy shear load, the main failure modes are yarn T tensile shear failure, matrix cracking and interface debonding. From Fig.8(c), it can be seen that the interface damage occurs first in the yarn/yarn contact zones near the right and left surfaces of the unit-cell at $\bar{\epsilon}_z = 0.38\%$. The interface damage in the unit-cell shows certain cut-edge effect. After $\bar{\epsilon}_z = 1.00\%$, the interface damage begins to occur in the yarn/yarn and yarn/matrix contact zones but the expansion rate is relatively slow. This is because of the load-bearing directional effect of the braiding yarns. That is, the stresses in different directional yarns are not balanced, which leads to the unbalanced stress distribution in the interface elements. Surely, this is obviously different from that under the tensile loads. For the debonded interface under compressive load, the frictional stress generates along the yarn axial direction and resists the micro-slip tendency of the fiber yarns. At this point, the shear stress on the debonded interface will

not immediately come to zero. Overall, under xy shear load, the shear stress components always play more important contribution to the damage evolution of interface. Under xz shear load, the main failure modes are yarn Z tensile shear failure, matrix cracking and interface debonding. The interface damage evolution process is presented in Fig. 8(d). It can be found that the whole process of interface damage initiation and evolution is similar to that under xy shear load, but the interface damage regions are changed due to the change of loading direction.

4.5 Parameter study

In meso-scale finite element modeling, the selection of suitable material parameters to accurately represent the mechanical response of the composites is very important and also very difficult. Interface stiffness, strength and friction coefficient are important interfacial parameters as they directly control and influence the mechanical behavior of interface and the mechanical properties of 3D braided composites. In this section, to understand how these interfacial parameters contribute to the effective stiffness and strength properties, numerical parameter studies are conducted by using the proposed modeling strategy.

4.5.1 Effect of interface stiffness on elastic properties of the composites

Fig. 9 represents the variation of the predicted elastic constants with interface stiffness. It is clearly seen from Fig. 9(a) that the elastic moduli of the material increase monotonically with the increase of interface stiffness. When K is small, the increase is significant. When K is greater than 1×10^5 , the increase is not obvious. As shown in Fig. 9(b), the Poisson's ratio μ_{xy} increases gradually with increasing the interface stiffness. In contrast, the Poisson's ratio μ_{zx} decreases gradually as the interface stiffness increases. Note that the changing tendencies are both significant when K is small. However, the effect of interface stiffness on the Poisson's ratios is relatively weak. It can be concluded that if the interface stiffness is small, the interface would be soft and easy to deform, which results in low prediction values of elastic modulus. Therefore, it is better to select a high value of interface stiffness in the appropriate range. For the zero-thickness interface cohesive element in 3D braided composite, $K \geq 1 \times 10^5$ is recommended.

4.5.2 Effect of interface strength on strength properties of the composites

In this section, the strength parameters of interface in Table 2 are termed as base strength S_0 . In order to study the effect of the interface strength on the strength properties of the 3D braided composites, six different interface strength conditions are employed. Fig. 10 depicts the variation of the predicted strengths with interface strength under four typical loading cases. It can be seen that, as compared to the shear strengths, the tensile strengths are prominently influenced by the interface strength. When the interface strength is less than $0.75S_0$, the tensile strengths, S_z and S_x , increase sharply as the interface strength increase. But when the interface strength is larger than $0.75S_0$, the increase of tensile strengths is very small and the curves become nearly horizontal lines. The shear strengths, S_{xy} and S_{xz} , increase gradually as the interface strength increase. However, the increments are not obvious even when the interface strength is very small. Since the braiding angle here is typical large, both the braiding yarn and interface elements bear the loads under tensile load while only the braiding yarn bears the main loads under shear load. Therefore, the interface damage has great influence on the load-bearing performance of the composites with large braiding angle under tensile load. But under shear load, the influence is not very

significant. Moreover, it should be pointed out that when the interface strength is relatively larger, the damage of interface elements becomes less under all the loading cases thus the variation of the predicted strength properties also becomes less.

4.5.3 Effect of interface friction coefficient on mechanical properties of the composites

The friction force will act when the interface element is damaged and the element is under compressive load, thus the interface friction coefficient has no effect to the predicted stiffness properties. By numerical discussion, it is found that the variation of the predicted strength properties with interface friction coefficient is very small, as given in Table 4. Under the external load, the stress state in the unit-cell model is complex. When the interface is damaged, parts of the interface elements are in compressive state. At this time, friction is introduced to enhance the shear toughness of fiber yarn thus improves the shear strength of the interface. However, even the friction has great influence on the mechanical properties of the interface, but in the unit-cell model, the number of damaged interface elements in compressive load only accounts for a small part of the overall interface elements. Furthermore, the interface friction effect is a meso-scale local performance while the strength is a macro-scale property, thus the effect of interface friction coefficient on the predicted strength properties of the composites is not significant.

In addition, it is also found that the critical fracture energy only has significant influence on the damage evolution of damaged interface elements but has little effect on the predicted stiffness and strength properties of the composites.

5 Conclusions

The mechanical properties of 3D braided composites under typical loading cases are numerically investigated from a new perspective. A meso-scale finite element model, in which the yarn/matrix and yarn/yarn interfaces are modeled by cohesive elements, is originally developed for that purpose. And then, the friction appearing on debonding interface is considered to propose a novel damage-friction combination constitutive model for the interface. Based on these, i.e. the continuum damage models of each constituent in conjunction with the meso-scale finite element modeling, the stiffness, strength and damage properties of 3D braided composites are analyzed. It is found that the load transfer, failure mode and damage mechanism are different under different loading cases as summarized below.

For interface, under tension loads, the load bearing of braiding yarn and interface elements is relatively balanced, and both the normal stress component and shear stress components contribute to the damage evolution of interface. Under shear loading, the load bearing of braiding yarn is related to the loading direction. The stresses distribution on the interface is not balanced and the shear stress components rule the damage evolution of interface. Since the reasonable interface constitutive model is introduced and the stress distribution and damage evolution of each constituent in the unit-cell can be obtained, the proposed model is useful for a good understanding of the mechanical response of all the constituent materials under typical loading cases. Furthermore, the effects of interface stiffness, interface strength and friction coefficient on the mechanical properties of composites are discussed in detail which provides a novel insight to the problem.

In addition, the results reported here in this paper may be helpful for designers to optimize and control the

interface performance of 3D braided composite structures.

Acknowledgements

This work was supported by Postdoctoral Science Foundation of Jiangsu Province (1402101C), Senior Talent Start-up Foundation of Jiangsu University (14JDG136), Jiangsu Government Scholarship for Overseas Studies and Jiangsu University Study-abroad Fund.

References

- [1] Wang YQ, Wang ASD. Microstructure/property relationships in three dimensionally braided fiber composites. *Compos Sci Technol* 1995; 53(2): 213-232.
- [2] Chen L, Tao XM, Choy CL. On the microstructure of three-dimensional braided preforms. *Compos Sci Technol* 1999; 59(3): 391-404.
- [3] Xu K, Xu XW. On the microstructure model of four-step 3D rectangular braided composites. *Acta Mater Compos Sin* 2006; 23(5): 154-160.
- [4] Li DS, Li JL, Chen L, et al. Finite Element Analysis of Mechanical Properties of 3D four directional Rectangular Braided Composites Part 1: Microgeometry and 3D Finite Element Model. *Appl Compos Mater* 2010; 17(4): 373-387.
- [5] Sun HY, Qiao X. Prediction of mechanical properties of three-dimensionally braided composites. *Compos Sci Technol* 1997; 57(6): 623-629.
- [6] Xu K, Xu XW. Finite element analysis of mechanical properties of 3D five-directional braided composites. *Mater Sci Eng A* 2008; 487(1-2): 499-509.
- [7] Zhang C, Xu XW. Finite element analysis of 3D braided composites based on three unit-cells models. *Compos Struct* 2013; 98:130-142.
- [8] Yu XG, Cui JZ. The prediction on mechanical properties of 4-step braided composites via two-scale method. *Compos Sci Technol* 2007; 67(3-4): 471-80.
- [9] Li DS, Fang DN, Jiang N, et al. Finite element modeling of mechanical properties of 3D five-directional rectangular braided composites. *Compos Part B* 2011; 42(6): 1373-1385.
- [10] Zeng T, Wu LZ, Guo L C. A finite element model for failure analysis of 3D braided composites. *Mater Sci Eng A* 2004; 366(1): 144-151.
- [11] Fang GD, Liang J, Wang BL. Progressive damage and nonlinear analysis of 3D four-directional braided composites under unidirectional tension. *Compos Struct* 2009; 89: 126-133.
- [12] Dong JW, Feng ML. Asymptotic expansion homogenization for simulating progressive damage of 3D braided composites. *Compos Struct* 2010; 92(4): 873-882.
- [13] Mahmood A, Wang X, Zhou C. Modeling strategies of 3D woven composites: A review. *Compos Struct* 2011; 93: 1947-1963.
- [14] Lu ZX, Xia B, Yang ZY. Investigation on the tensile properties of three dimensional full five directional braided composites. *Comput Mater Sci* 2013; 77: 445-455.
- [15] Zhang DT, Sun Y, Wang XM, et al. Meso-scale finite element analyses of three-dimensional five-directional braided composites subjected to uniaxial and biaxial loading. *J Reinf Plast Comp* 2015; 34(24): 1989-2005.
- [16] Fang GD, Liang J, Wang BL. Effect of interface properties on mechanical behavior of 3D four directional

braided composites with large braid angle subjected to uniaxial tension. *Appl Compos Mater* 2011; 18(5): 449-465.

[17] Xu YJ, You T, Du CL. An integrated micromechanical model and BP neural network for predicting elastic modulus of 3-D multi-phase and multi-layer composites. *Compos Struct* 2015; 122: 308-315.

[18] Lei B, Liu Z G, Ya J X, et al. Bearing abilities and progressive damage analysis of three dimensional four-directional braided composites with cut-edge. *Appl Compos Mater*, 2016, 23(4): 839-856.

[19] Lu ZX, Wang CY, XiaB, et al. Effect of interfacial properties on the uniaxial tensile behavior of three-dimensional braided composites. *Comput Mater Sci* 2013; 79: 547-557.

[20] Xu Q, Tao WM, Qu SX, et al. A cohesive zone model for the elevated temperature interfacial debonding and frictional sliding behavior. *Compos Sci Technol* 2015; 110: 45-52.

[21] Sharma R, Mahajan P, Mittal RK. Elastic modulus of 3D carbon/carbon composite using image-based finite element simulations and experiments. *Compos Struct* 2013; 98: 69-78.

[22] Li XT, Binienda WK, Goldberg RK. Finite-element model for failure study of two-dimensional triaxially braided composite. *J Aerosp Eng* 2010; 24(2):170-180.

[23] Zhang C, Li N, Wang WZ, et al. Progressive damage simulation of triaxially braided composite using a 3D meso-scale finite element model. *Compos Struct* 2015; 125: 104-116.

[24] Wang C, Zhong YC, Adaikalaraj PF, et al. Strength prediction for bi-axial braided composites by a multi-scale modelling approach. *J Mater Sci* 2016; 51: 6002-6018.

[25] Camanho PP, Davila CG. Mixed-mode decohesion finite elements for the simulation of delamination in composite materials. 2002; NASA/TM-2002-211737.

[26] Alfano G, Sacco E. Combining interface damage and friction in a cohesive-zone model. *Int J Numer Methods Eng* 2006; 68: 524-582.

[27] Hashin Z. Failure criteria for unidirectional fiber composite. *J Appl Mech* 1980; 47: 329-334.

[28] Lapczyk I, Hurtado JA. Progressive damage modeling in fiber reinforced materials. *Compos Part A* 2007; 38(11): 2333-2341.

[29] Xia ZH, Zhang YF, Ellyin F. A unified periodical boundary conditions for representative volume elements of composites and applications. *Int J Solids Struct* 2003; 40(8): 1907-1921.

[30] Li SG. Boundary conditions for unit cells from periodic microstructures and their implications. *Compos Sci Technol* 2008; 68(9): 1962-1974.

[31] Zhang C, Curiel-Sosa JL, Bui TQ. Comparison of periodic mesh and free mesh on the mechanical properties prediction of 3D braided composites. *Compos Struct* 2017; 159: 667-676.

[32] Chamis CC. Mechanics of composites materials: past, present and future. *J Compos Tech Res* 1989; 11(1): 3-14.

[33] Curiel Sosa JL, Souza Neto EA, Owen DRJ. A combined implicit-explicit algorithm in time for nonlinear finite element analysis. *Commun Numer Meth Eng* 2006; 22: 63-75.

[34] Curiel Sosa JL, Beg OA, Liebana Murillo JM. Finite element analysis of structural instabilities using a switching implicit/explicit technique. *Int J Compu Meth Eng Sci Mech* 2013; 14(5): 452-464.

List of Figure Captions

Fig. 1 Bilinear constitutive model of interface element under pure mode (a) mode I (b) mode II or mode III

Fig. 2 Mix-mode bilinear constitutive model of interface element

Fig. 3 Unit-cell structural model of 3D braided composites (a) 3D model of unit-cell (b) Topological relationship of braiding yarns

Fig. 4 Finite element mesh of unit-cell of 3D braided composites (a) Unit-cell mesh (b) Interface mesh

Fig. 5 Flow chart of numerical analysis process

Fig. 6 Comparison of numerical results adopted by cohesive constitutive model (left) available in ABAQUS and VUMAT subroutine (right) developed in this paper (a) Stress station (b) Damage distribution

Fig. 7 The computed stress-strain curves

Fig. 8 Damage evolution process of interface element in unit-cell model under typical loadings

Fig. 9 Variation of the predicted elastic constants with interface stiffness

Fig. 10 Variation of the predicted strengths with interface strength

Table 1 Material properties of fiber and matrix

| | E_{11} (GPa) | E_{22} (GPa) | G_{12} (GPa) | G_{23} (GPa) | μ_{12} | X_T (MPa) | X_C (MPa) | S (MPa) | G_f (N/mm) | G_m (N/mm) |
|--------|----------------|----------------|----------------|----------------|------------|-------------|-------------|-----------|--------------|--------------|
| T300 | 230 | 40 | 24 | 14.3 | 0.26 | 3528 | 2470 | | 8.0 | |
| Matrix | 3.5 | | | | 0.35 | 80 | 241 | 80 | | 1.5 |

Table 2 Properties of interface elements

| K (N/mm ³) | N (MPa) | $S=T$ (MPa) | G_{IC} (N/mm) | $G_{IIC} = G_{IIIC}$ (N/mm) |
|--------------------------|-----------|-------------|-----------------|-----------------------------|
| 1×10^6 | 80 | 60 | 0.306 | 0.632 |

Table 3 Predicted stiffness and strength properties

| Elastic modulus (Gpa) | Prediction | Poisson's ratio | Prediction | Strength (MPa) | Prediction |
|-----------------------|------------|-----------------|------------|----------------|------------|
| E_x | 10.53 | μ_{xy} | 0.30 | S_x | 70.55 |
| E_y | 10.53 | μ_{zx} | 0.42 | S_y | 70.15 |
| E_z | 17.46 | μ_{zy} | 0.42 | S_z | 134.37 |
| G_{xz} | 17.86 | | | S_{xz} | 212.67 |
| G_{yz} | 17.86 | | | S_{yz} | 209.96 |
| G_{xy} | 11.55 | | | S_{xy} | 161.48 |

Table 4 Predicted strength properties with different friction coefficients

| Friction coefficient | S_x | S_z | S_{xy} | S_{xz} |
|----------------------|-------|--------|----------|----------|
| $\mu=0.0$ | 70.55 | 134.37 | 161.48 | 212.67 |
| $\mu=0.5$ | 70.83 | 134.47 | 162.93 | 214.03 |
| $\mu=1.0$ | 70.87 | 134.58 | 163.62 | 214.13 |